Chapter 2

THERMALLY-ACTIVATED SHAPE MEMORY BEHAVIOR OF DIFFERENT NANOCOMPOSITES BASED ON ETHYLENE COPOLYMERS.

Valentina Sessini[1], David Brox[1-2], Antonio Julio López[2], Alejandro Ureña[2], Jean-Marie Raquez*[3], Philippe Dubois[3], José M. Kenny[1] and Laura Peponi*[1]

[1] Instituto de Ciencia y Tecnología de Polímeros, ICTP-CSIC, Spain
[2] Departamento de Matemática Aplicada, Ciencia e Ingeniería de Materiales y Tecnología Electrónica. Universidad Rey Juan Carlos, Spain
[3] Laboratory of Polymeric and Composite Materials, University of Mons, Belgium

ABSTRACT

Shape memory materials are able to change their shape upon application of an external stimulus such as temperature, humidity, light, electric or magnetic fields, etc. This chapter focuses on nanocomposites systems with shape memory response due to their high scientific and technological relevance.. In particular, three different nanocomposites based on ethylene copolymers are presented with different thermally-activated mechanisms such as Nucrel® and Surlyn® reinforced with Silica nanoparticles, blends of EVA/thermoplastic starch reinforced with natural bentonite and EVA reinforced with SNCs. All of these systems present shape memory ability, evidencing how the addition of well dispersed nanoparticles can affect the shape memory response of the neat matrix.

Keywords: Ethylene copolymers, ionomeric resin, Nucrel®, Surlyn®, stimuli-responsive, shape memory, thermally-activated, nanocomposites.

* Corresponding Author address
Email: lpeponi@ictp.csic.es; jean-marie.raquez@umons.ac.be

INTRODUCTION

Smart materials have the capability to respond to an external stimulus. Between smart materials, there is a class of polymers known as shape memory polymers (SMPs), able to change their shape by fixing a temporary one upon the application of an external stimulus [1]. Moreover, shape memory materials have the ability to recover the original shape once the external stimulus is applied again.

Shape memory process in polymers involves the retention of the deformation entropy as internal energy and its activation due to an external stimulus, which means the relaxation of the polymer chains and therefore, the recovery of the original shape [2]. To obtain this response, a particular polymer structure is needed and viscoelastic relaxation is necessary to create an elevated mobility to the macromolecular chains.

Different are the external stimuli able to produce the shape change in the polymeric materials, such as temperature [3-7], humidity [8, 9], pH [10], light [11] and electric or magnetic field [12]. However, thermal stimulus is the most common one [13-15]. In general, the shape memory mechanism in the SMPs encompasses two main stages: the programming stage and the recovery stage as schematically shown in Figure 1. In the first stage, a temporary shape (shape B) is fixed by the application of an external stimulus. In the second stage, the original shape is recovered (shape A) after applying the same stimulus as can be seen in Figure 1 [16].

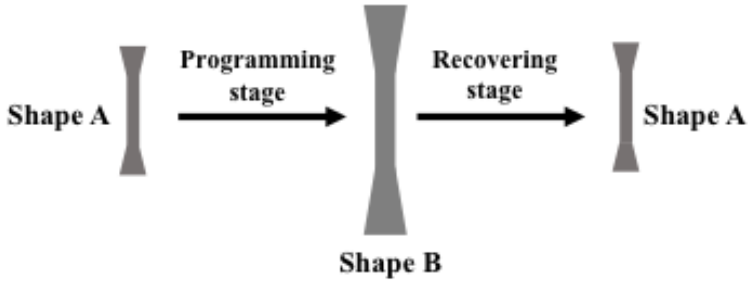

Figure 1. Scheme of the shape memory process.

Moreover, shape memory polymers are formed by two different phases: the reversible phase, also called "switching phase", which is able to fix the temporary shape and the "permanent phase", responsible for recovering the original shape of the polymeric material (Figure 1). Both phases can be formed by chemical or physical domains, affecting the thermal response of the polymeric materials. The external stimulus, such as temperature, can fix the temporary shape and counteracts the elastic forces, which tend to return the material to its original shape [17]. This is the reason why a reversible thermal

transition to a specific temperature (T_{trans}) is needed. In particular, permanent bonds are retained at temperatures higher than T_{trans}, while reversible and permanent domains are both present at temperatures lower than T_{trans} [18].

The above-mentioned SMPs are the most common ones and they are usually referred as "one-way shape memory polymers", with two active phases – i.e the switching and the permanent domains – with an external stimulus triggering the change from one shape to another, Figure 1.

In general, shape memory properties are characterized by thermomechanical cycle experiments [19, 20]. Figure 2 shows a 3D representation of a thermo-mechanical shape memory cycle.

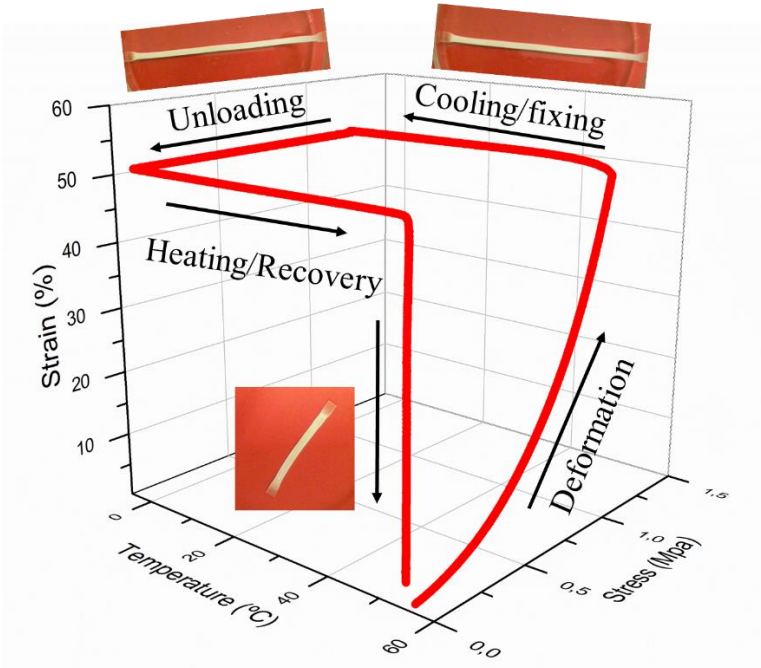

Figure 2. Scheme of 3D thermo-mechanical shape memory cycle.

The curve shows the process starting with a deformation of the sample at the switching temperature (T_{sw}). Afterwards, a quick cooling stage is done to temperature lower than T_{trans} (fixing temperature, T_{fix}) maintaining the applied load until the temporary shape is fixed. After, unloading of the applied stress is followed by an increase of the temperature above T_{trans} (T_{sw}) to activate the recovery of the permanent shape.

When the polymer shows two temporary shapes and only one permanent shape, it is known as "triple" shape memory polymer [21]. These polymers need one programming stage, to program both temporary shapes, and two different

triggers to recover firstly the intermediate temporary shape and subsequently the original one, as schematically shown on Figure 3.

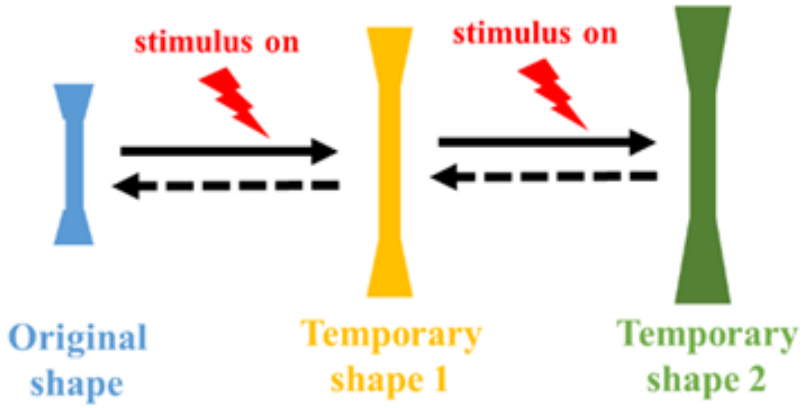

Figure 3. Scheme of triple shape memory process.

Therefore, depending on the chemical or physical structure of the switching domains, the melting temperature, T_m, or the glass transition temperature, T_g, will be considered as the T_{trans} [22].

In particular, in semicrystalline polymers, T_m is used as T_{trans}. Polymers with chemical crosslinking, i.e., covalent or thermoreversible bonds [23] or physically crosslinked by means of segregated domains [24] or a mixture of both types forming copolymers [25] are representative of SMPs constructed around T_m. In general, in the copolymers the phase with higher T_{trans} is the responsible for the preservation of the physical structure, maintaining the permanent shape. Meanwhile, the phase with the lower T_{trans} is the responsible for the fixation of the temporary shape [26] as shown in the next paragraphs of this chapter. When SMPs are based on T_g, they are able to fix a temporary shape to a temperature below their T_g and to recover the permanent one above this temperature [18].

It is important to note also that in the last years shape memory nanocomposites [27] have obtained a great interest from both academic and industrial sectors studying the incorporation of nanofillers such as carbon nanotube, layered silicates, titanium oxide, etc., into the polymer matrix [28]. The addition of nanoparticles, characterized by high surface area, and the obtention of favorable interactions between the matrix and the nanofillers, result in the improvement of numerous properties including thermal stability, flame retardancy, mechanical properties, gas barrier properties, and so on as compared with neat polymers [29].

Moreover, in recent years, nanowhiskers and nanocrystals prepared from natural polymers, such as cellulose and starch, have been applied to reinforce biodegradable or non-biodegradable polymeric matrix [13, 30-33]. In

particular, starch is an abundant biopolymer, which is totally biodegradable. Starch nanocrystals (SNCs) have been used as fillers in polymeric matrices such as natural rubber [34], poly-vinyl alcohol [35] and thermoplastic starch [36]. The physical properties of the resulting nanocomposites were improved by the incorporation of SNCs [37].

Copolymers of ethylene-vinyl acetate (EVA) are a class of widely used polymers, with a variety of industrial applications such as flexible packaging, membranes, cable and wire, hose and tube, photovoltaic encapsulants, footwear and biomedical applications [38-40]. Recent developments in the field of shape memory polymers have drawn increasing attention to EVA copolymers for potential non-structural applications (microfluidic devices, soft actuators etc.). However, most of the studies reported in literature of the shape memory behavior of EVA are about crosslinked EVA [41-43]. Nevertheless, Wu et al. reported the study of the shape recovery of a commercial EVA by studying its creep and the thermo-responsive shape memory effect presenting two potential application [44].

However, in many cases, EVA application is limited due to its low tensile strength, thermal stability, and high flammability [28, 45]. To overcome these deficiencies, commonly either the vinyl acetate (VA) content of EVA varies or suitable nanofillers are incorporated in the EVA matrix. Indeed, varying the VA content, many properties of EVA change while the polar groups of vinyl acetate could get involved with a strong interaction with nanofillers, making its dispersion homogeneous. In this regard, several investigations have been reported in literature, including the incorporation of graphite oxide [46], sepiolite [47], montmorillonite [39, 48], carbon nanotube [49], and so on.

Poly(ethylene-co-methacrylic acid) copolymer, named Nucrel® and its sodium neutralized counterpart with the tradename of Surlyn® are manufactured by Dupont^{Tm} Company. The self-healing properties of ionomeric resin under high speed impact, i.e. ballistic damage [50, 51], and even under hyper-velocity impacts (1-4 km/s) simulating space debris impacts [52] has been studied.

This ionomer has ionic groups integrated by the carboxyl groups of the polymer that create strong interactions by coulombic potentials between the ionic charges, forming what it are called ionic clusters. These clusters are able to form reversible ionic networks [53] and the inter-chain interactions designed the permanent network. Due to the presence of two different phases in these polymers, it is possible to use them for designing shape memory polymers.

In this chapter, different nanocomposites based on ethylene copolymers are presented with different mechanisms used to obtain the shape memory response.

In particular three different systems are studied based on Nucrel® and Surlyn® reinforced with Silica nanoparticles, blends of EVA/thermoplastic starch reinforced with natural bentonite and EVA reinforced with SNCs.

Thermally-activated shape memory characterization

Thermally-activated shape memory behaviour of our nanocomposites was studied through thermo-mechanical cycle experiments using an Instron Universal Testing Machine equipped with a temperature chamber. For each material, the right transition or switching temperature and the fixing temperature were found based on the thermal and dynamo-mechanical characterization.

Therefore, with the aim to get a quantitative estimation of the shape memory properties of the materials, the strain fixity ratio (R_f) and the strain recovery ratio (R_r) have been calculated [20]. In particular, R_r, the ability to recover the initial shape, was taken as the ratio of the recovered strain to the total strain, as given by the following equation:

$$R_r(N) = \frac{\left(\varepsilon_m - \varepsilon_p(N)\right)}{\varepsilon_m - \varepsilon_p(N-1)} \times 100\ \% \qquad \text{Equation (1)}$$

R_f, the ability to fix the temporary shape, is the amplitude ratio of the fixed strain to the total strain, as presented by the Equation 2:

$$R_f(N) = \frac{\varepsilon_u(N)}{\varepsilon_m} \times 100\ \% \qquad \text{Equation (2)}$$

where, ε_m is the deformed strain, ε_u the fixed strain, ε_p the recovered strain and N is the number of cycles.

Poly(ethylen-co-methacrylic acid) random copolymer and ionomers

Commercial poly(ethylen-co-methacrylic acid) random copolymer (EMAA) named Nucrel® 960 (containing 15 wt % of methacrylic acid (MAA) comonomer) and its ionomer, Surlyn® 8940, with 30 % of the MAA comonomer neutralized by sodium (EMAA-Na), were kindly provided by Dupont^{Tm} Company. Silicon Dioxide Nanopowder (SiO_2) with a particle average size of 7-14 nm and specific surface higher than 200 m^2/g was supplied by EMFUTUR.

Shape memory properties of a commercial poly(ethylen-co-methacrylic acid) random copolymer named Nucrel® 960 and its ionomeric resin, Surlyn® 8940, were studied. With the purpose of select the parameters for thermo-mechanical cycles, dynamic thermo-mechanical analysis was performed in order to study the main chain relaxation of the materials. Tanδ curves are reported in Figure 4 for Nucrel® as well as Surlyn®. Both materials have similar elastic properties. Nucrel® showed three main relaxations in the range of temperature between -140 and 100 °C. In particular, around -70 ºC a relaxation was observed and it was ascribed to the local molecular motion of the amorphous segment of PE while at ~ 30 ºC the relaxation corresponding to the melting of the secondary crystals of PE was detected. Moreover, after ~ 70 ºC the relaxation corresponding to the primary crystallites of PE was observed [54, 55]. For Surlyn®, the same relaxations were detected but the relaxation below 0 ºC were more evident and were ascribed not only to the molecular motion of the amorphous phase of PE but also to the ion-depleted in the amorphous region, although different explanation have been proposed in literature for this relaxation over the year [56]. The relaxation corresponding to the melting of the secondary crystals of PE was shifted to higher temperature for Surlyn® (~ 60 ºC) as well as that one of the primary crystals, starting from ~ 85 ºC. In this case, three types of physical crosslinks are present due to the ionic domains, primary and secondary polyethylene crystallites. Above 100 ºC, where all the polyethylene crystals have melted, the Surlyn® is a physically crosslinked rubber with a supramolecular network formed by ionic interactions [57].

Polyethylene crystals provide the temporary network, so the switching temperature for shape memory is determined by their melting temperature. In order to compare the shape memory properties of both Nucrel® and Surlyn® and their nanocomposites reinforced with 1 wt % of silica nanoparticles, a common switching temperature was taken, that is, at 60 ºC. Thus, the crystallites that melt below 60 °C (mainly the secondary crystallites) are used as the temporary network for generating shape memory effect. In particular, For Nucrel® the permanent shape is achieved through the largest and

strongest primary *polyethylene* crystals that create a physical network with the amorphous chains of the material. While for Surlyn®, the presence of the Na^+ ions allows to obtain a more stable permanent network due to the presence of the ionomeric aggregates in addition to the physical network formed by the PE primary crystals.

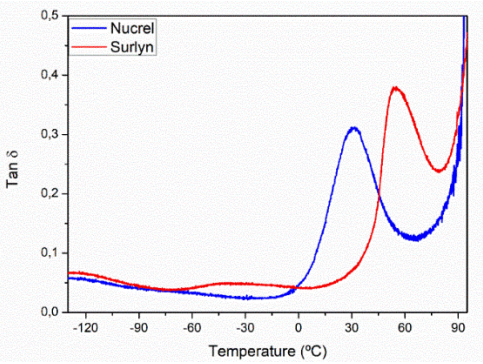

Figure 4. Damping factor (Tanδ) as a function of temperature for both Nucrel® and Surlyn®.

Once the T_{sw} was selected, the mechanical response of our materials was studied at that temperature (60°C). A stress-strain test (Figure 5) was carried out to determine the maximum deformation that the material could withstand at the T_{sw}.

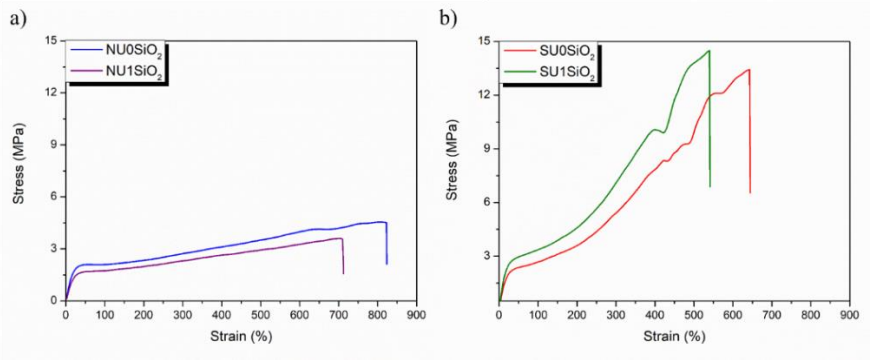

Figure 5. Stress-strain curves performed at 60 °C for the neat materials and their respective nanocomposites. a) Nucrel® and b) Surlyn®.

In Figure 5, it is possible to easy notice that Surlyn® showed different mechanical properties compared to Nucrel®. In fact, Surlyn® showed higher elastic modulus and higher maximum stress, while the elongation at break decreased for Surlyn® due to the Na^+ neutralization of methacrylic acid groups. The presence of SiO_2 improve the mechanical properties of both neat materials, Nucrel® and Surlyn®. Even if the elongation at break decreased due to the

ionomer structure as well as to the presence of SiO_2 in both matrices, the maximum deformation at 60 ºC for the shape memory test was higher than 500 % for all the materials. Thermally-activated shape memory properties were studied using an Instron Machine equipped with a temperature chamber. Samples for the thermo-mechanical cycles were cut from compression-molded films into rectangular specimens of approximately 20 mm x 5 mm x 0.50 mm. The samples were heated at the T_{sw} of 60 ºC for 5 min, followed by a strain-controlled uniaxial stretching applied until a fixed percentage of deformation, i.e., 50 % and 100 %. They were then quenched at 0 ºC (T_{fix}) under the same constant stress, which after 10 minutes was released. A free-strain recovery was then performed at the selected T_{sw}. The 2D stress-strain and 3D thermo-mechanical stress-strain-temperature cycle diagrams for neat Nucrel® and its nanocomposite counterpart are shown in Figure 6 and Figure 7 at 2 different deformation values, 50 % and 100%. In order to evaluate the repeatability of the shape-memory properties, four thermo-mechanical cycles were completed for each sample.

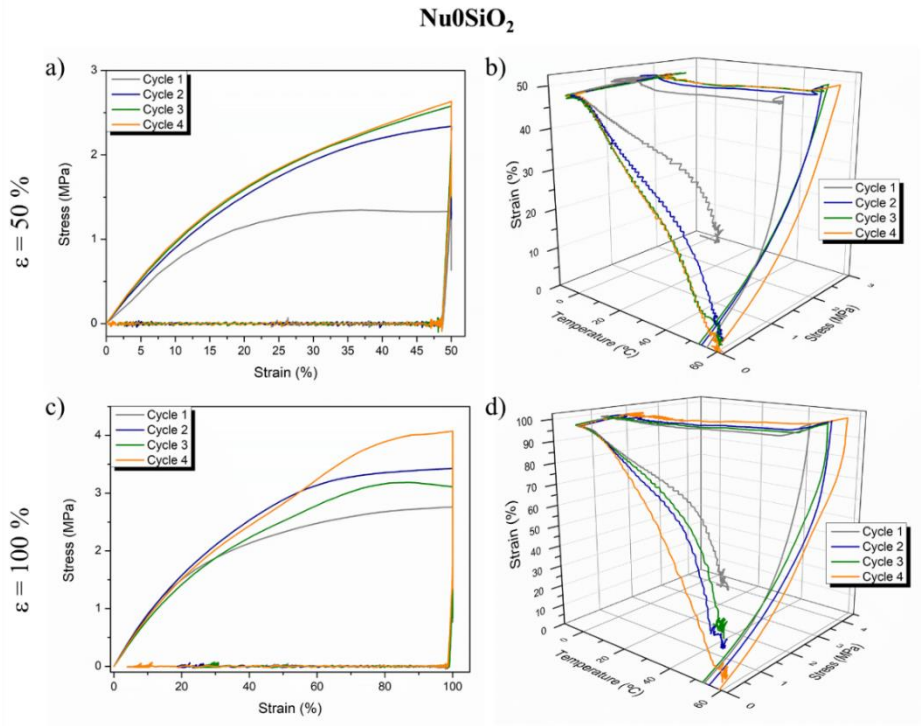

Figure 6. Thermo-mechanical cycles for neat Nucrel®. 2D stress-strain cycles and 3D stress-strain-temperature cycle diagrams at 50 % (a-b) and 100 % (c-d) of deformation.

All the samples shown a good ability to fix the deformed shape at the selected T_{fix} while the recovery process begun before reaching the selected T_{sw},

as it was expected by observing Figure 4, where the peak related to the melting of PE secondary crystals is at around 25 °C. Moreover, it is possible to notice that increasing the number of cycles, the stress needed to reach the same value of elongation (50 % or 100 %) is higher than the stress applied during the first cycle. This is probably due to a reorganization of the polymeric structure after the first cycle.

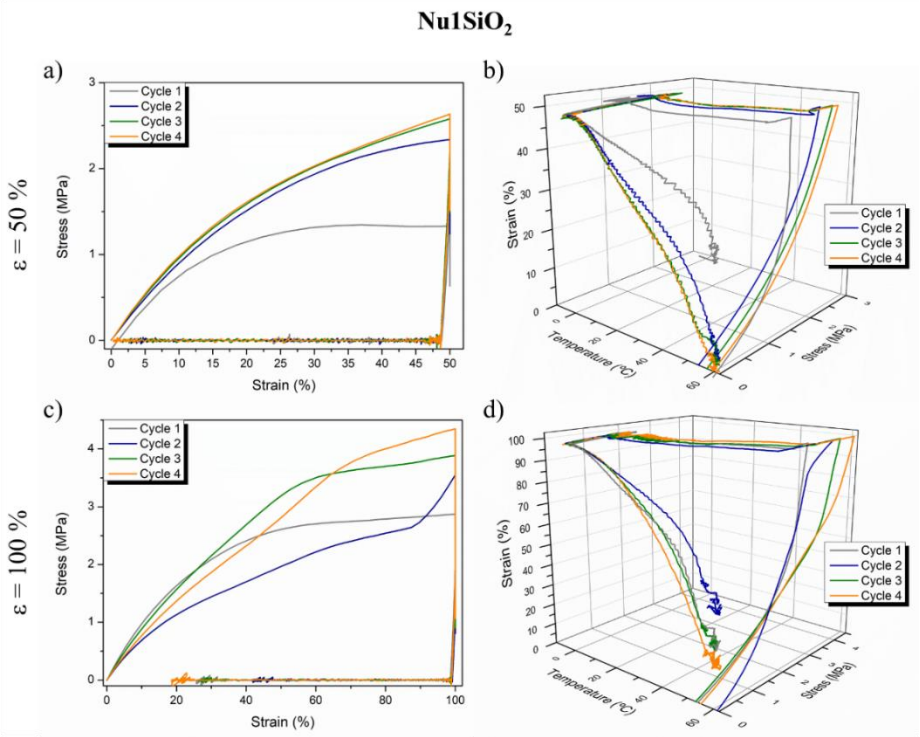

Figure 7. Thermo-mechanical cycles for Nucrel® nanocomposite reinforced with 1 wt % of SiO_2. 2D stress-strain cycles and 3D stress-strain-temperature cycle diagrams at 50 % (a-b) and 100 % (c-d) of deformation.

In Table 1, the results of thermo-mechanical cycles in terms of R_r and R_f are summarized for Nucrel® and its SiO_2 reinforced nanocomposite. Between the samples based on Nucrel®, we can conclude that higher values of R_r were observed for a deformation of 50 % and in particular for the sample reinforced with 1 wt % of SiO_2. In fact, for 100 % of deformation the R_r values were drastically dropped towards lower values compare with that obtained for 50 % of deformation. Furthermore, R_r values improved increasing the number of cycles. This is probably due to a progressive rearrangement of the polymeric structure cycle by cycle, until reaching a constant value. Whereas the R_f values are higher for the sample reinforced with silica nanoparticle for both applied deformations. The presence of silica nanoparticle increase the ability to fix the temporary shape, probably due to a decrease of the polymeric chain mobility.

Thermo-mechanical cycles were performed also for the samples based on Surlyn® following the same procedure than Nucrel®.

Table 1. Values of R_r and R_f obtained by thermo-mechanical cycles at 50 % and 100 % of deformation for Nucrel® and its SiO_2 nanocomposite.

Sample	**Ɛ (%)**	**R_r (%)**				**R_f (%)**			
		1	2	3	4	1	2	3	4
NU0SiO_2	50	81	74	96	97	97	97	95	97
	100	55	81	73	93	99	99	99	98
NU1SiO_2	50	59	94	96	98	99	97	95	97
	100	73	59	74	81	99	99	99	99

The 2D stress-strain and 3D thermo-mechanical stress-strain-temperature cycle diagrams for neat Surlyn® and its nanocomposite counterpart are shown in Figure 8 and Figure 9 at 2 different deformation values, 50 % and 100 %.

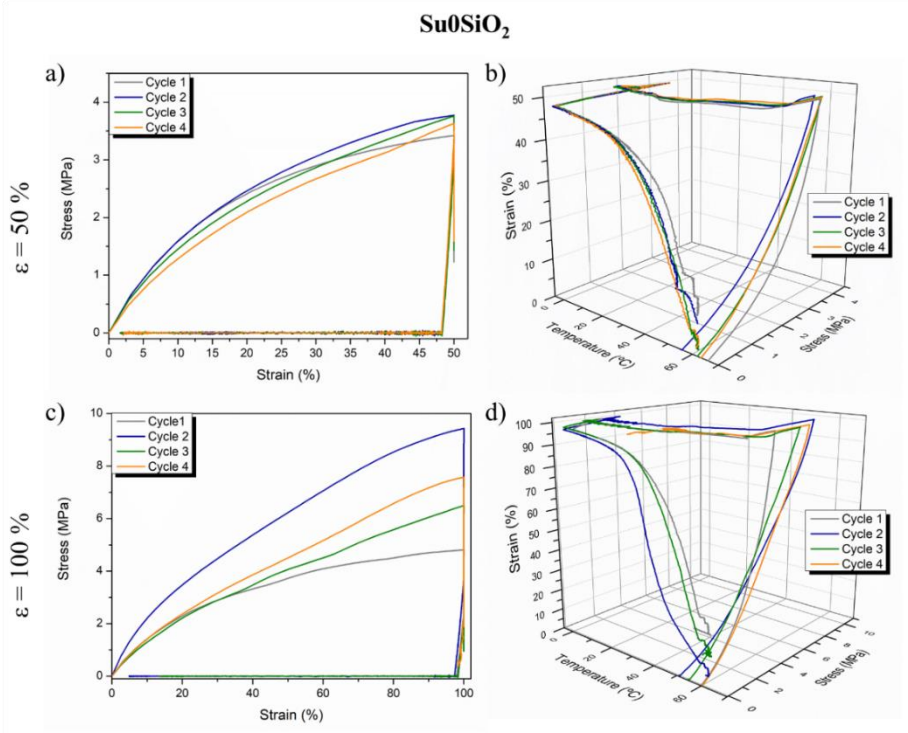

Figure 8. Thermo-mechanical cycles for neat Surlyn®. 2D stress-strain cycles and 3D stress-strain-temperature cycle diagrams at 50 % (a-b) and 100 % (c-d) of deformation.

As noted for Nucrel® based materials also the samples based on Surlyn® shown a good ability to fix the deformed shape at the selected T_{fix}. Compared with Nucrel®, Surlyn® based materials are more stable during the recovery,

maintaining the temporary shape longer but not until the selected T_{sw}, as was expected observing Figure 4, where the peak related to the melting of PE secondary crystals is at around 60 °C. Moreover, it is possible to notice that increasing the number of cycles, the stress needed to reach the same value of elongation is higher than the stress applied during the first cycle when 100 % of elongation was applied. On the contrary, when 50 % of elongation was applied, the value of applied stress was almost constant during the different cycles. This is probably due to the strongest physical network formed by ionomeric interaction in Surlyn®

.

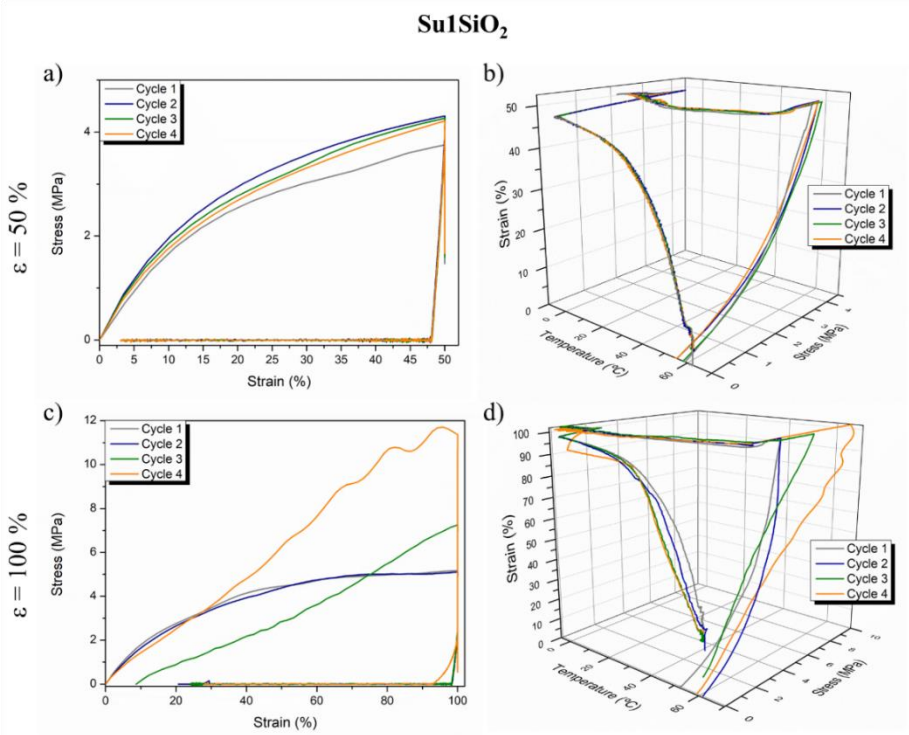

Figure 9. Thermo-mechanical cycles for Surlyn® nanocomposite reinforced with 1 wt % of SiO_2. 2D stress-strain cycles and 3D stress-strain-temperature cycle diagrams at 50 % (a-b) and 100 % (c-d) of deformation.

In Table 2, the results of thermo-mechanical cycles in terms of R_r and R_f are summarized for Surlyn® and its SiO_2 reinforced nanocomposite.

Table 2. Values of R_r and R_f obtained by thermo-mechanical cycles at 50 % and 100 % of deformation for Surlyn® and its respective nanocomposite.

Sample	**Ɛ (%)**	**R_r (%)**				**R_f (%)**			
		1	2	3	4	1	2	3	4

$SU0SiO_2$	50	81	85	96	95	97	96	97	96
	100	76	95	86	88	98	97	98	97
$SU1SiO_2$	50	86	93	93	94	96	96	98	96
	100	70	79	78	72	98	98	98	92

As observed for Nucrel®, higher values of R_r were observed for 50 % of deformation also for the samples based on Surlyn®, in particular for the sample reinforced with 1 wt % of SiO_2. Compared with Nucrel®, the decrease of the R_r values when 100 % of deformation is applied, was less evident due to the higher mechanical properties of Surlyn® thanks to the ionomeric network. However, R_r values improved after increasing the number of cycles. Moreover, the R_f values are pretty much the same for neat sample as well as for the sample reinforced with silica nanoparticle.

Poly(ethylene-co- vinyl acetate) random copolymer/thermoplastic starch blends and nanocomposites.

Native pea starch was used as received to obtain thermoplastic starch (TPS). Commercial EVA copolymer with 19 wt % VA content was purchased from Exxon Mobil Chemical Company. Glycerol (purity 97 %) was used as starch plasticizer and commercial natural bentonite, Cloisite-Na^+ ($CLNa^+$), with a typical dimension, ranging from 2 to 13 μm was used as nanofillers.

In our previous work [40], the thermally-activated shape memory effect of neat ethylene-vinyl acetate copolymer and its blends with thermoplastic starch has been studied by using the stretch-induced crystallization mechanism to program the temporary shape. In particular, two different blends with different TPS content, i.e., 40 and 50 wt %, have been tested and compared with neat EVA, as well as EVA/TPS blends based nanocomposites reinforced with 1 wt % of natural bentonite, ($CLNa^+$). Indeed was demonstrated that a new poorly organized crystalline structure (A phase), induced by stretching the sample until 250 % of elongation, was used as switching phase of EVA. Therefore, the melting temperature of the crystalline phase A was considered the switching temperature of our system. The presence of the two different crystal phases in EVA was first confirmed by DSC analysis using the same programming condition used for the shape memory activation, i.e., after stretching 250 % of elongation at 40 ºC. The DSC thermograms related to the first heating scan of non-stretched and stretched samples, blends and their nanocomposites are showed in Figure 10.

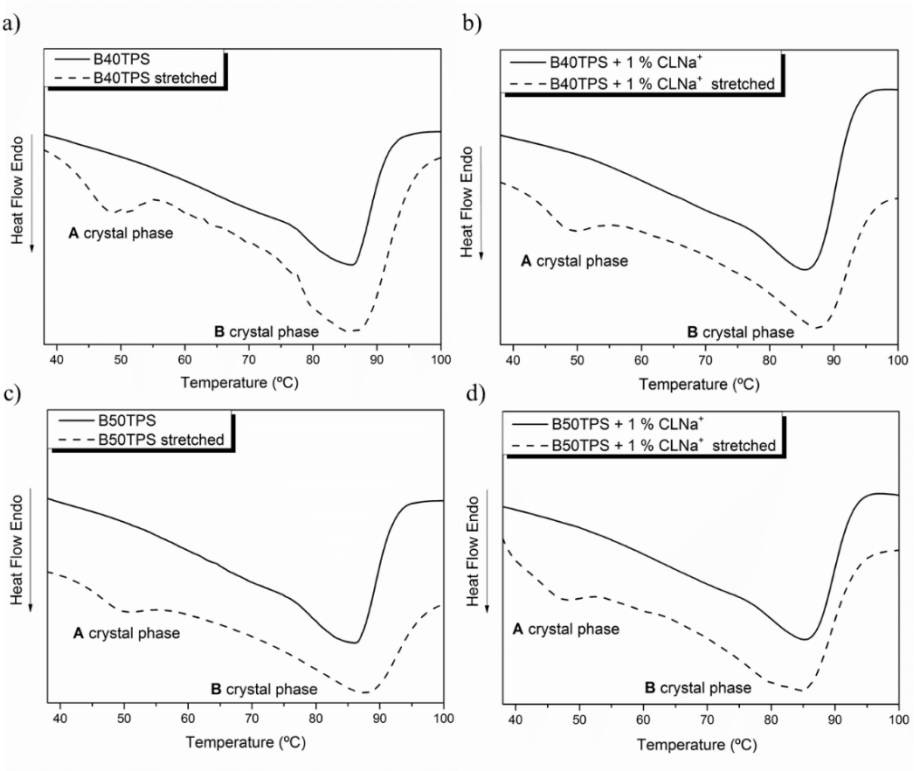

Figure 10. First cycle DSC thermograms for non-stretched and stretched blends and their nanocomposites: a) B40TPS, b) B40TPS + 1 % $CLNa^+$, c) B50TPS and d) B50TPS + 1 % $CLNa^+$.

It easy to note that, as for pure EVA [40], while both non-stretched blends and nanocomposites present only B-phase crystals, a new crystalline phase with a T_m of about 50 °C is presented after stretching the EVA-based samples. Thus, the desired two different crystal phases A and B were obtained in these EVA-based materials. Therefore, the new induced crystal phase A is the phase responsible for fixing the temporary shape of our system while amorphous EVA, thermoplastic starch and B crystal phase network was that responsible for memorize the original shape, as reported in our previous work [40]. When the heating is applied, the crystalline phase A melts and the system recovers its permanent shape.

The thermally-activated shape memory properties of neat EVA, the blends and their nanocomposites were characterized by Instron Machine. In brief, the parameter employed were 40 ºC as stretching temperature (T_s), 250 % of elongation, T_{fix} = 10º C and 60 ºC as T_{sw}. 3D thermo-mechanical stress-strain-temperature cycles and the 2D stress-strain diagram were determined for all the samples studied (Figure 11). In order to evaluate the repeatability of the shape-

memory properties, five different thermo-mechanical cycles were performed for each sample.

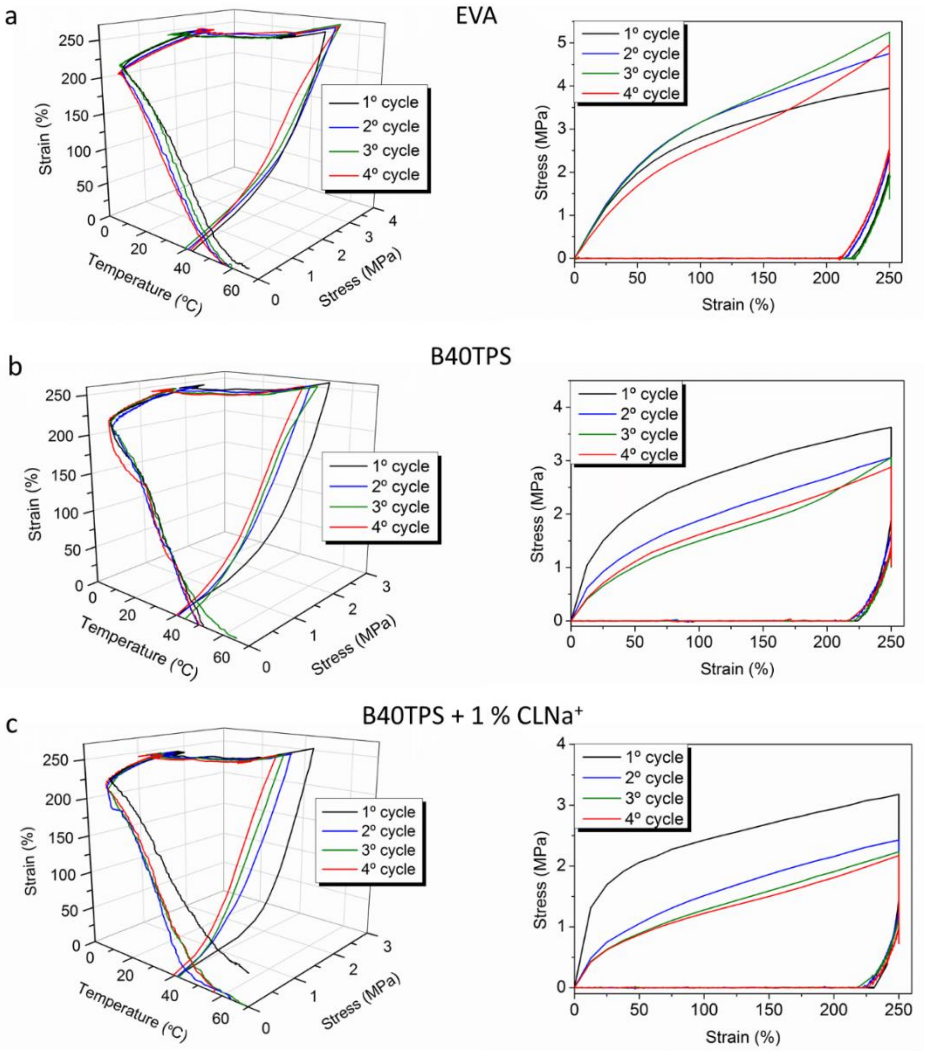

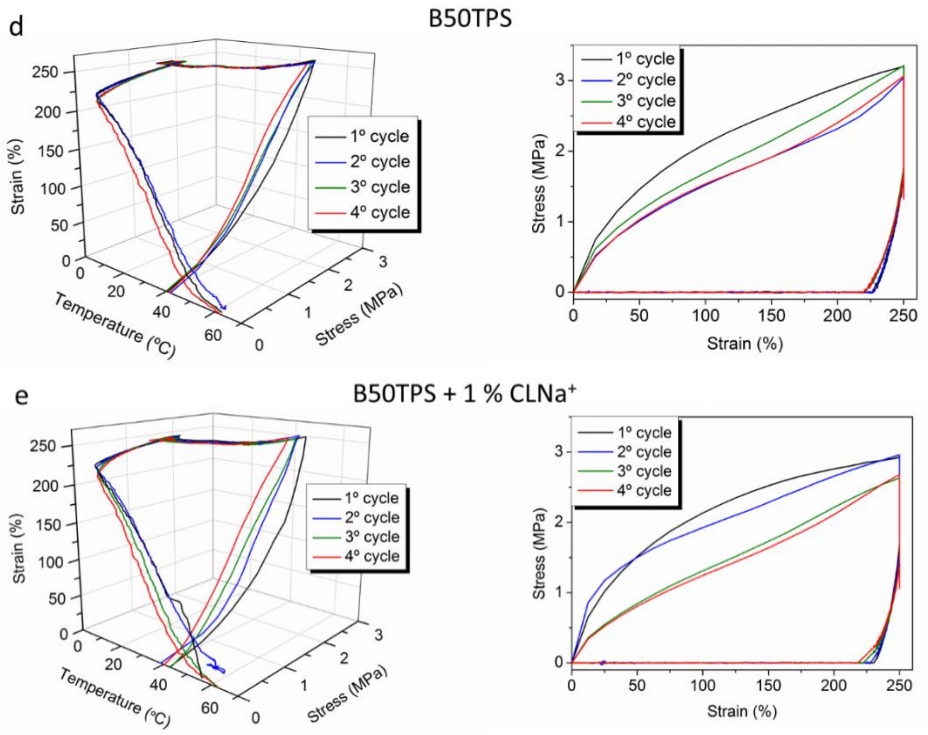

Figure 11. 3D thermo-mechanical stress-strain-temperature cycle and the 2D stress-strain diagram for (a) Neat EVA, (b) B40TPS, (c) B40TPS + 1 % $CLNa^+$, (d) B50TPS, (e) B50TPS + 1 % $CLNa^+$. Reprinted with permission from (Sessini V, Raquez J-M, Lo Re G, et al. Multiresponsive Shape Memory Blends and Nanocomposites Based on Starch. ACS applied materials & interfaces. 2016 2016/08/03;8(30):19197-19201) [40]. Copyright 2016 American Chemical Society.

The values obtained in every cycle for both the R_r and the R_f are summarized in Table 3. The results show that the presence of TPS did not affect the induced thermo-responsive mechanism of EVA.

The values reflect that the ability to recover the initial shape is excellent, showing R_r values higher than 90 %. Moreover, the very high EVA ability to fix the temporary shape during the first cycle slightly decreases during the following thermo-mechanical cycles from 99 % to 85 %. When the TPS is added, the R_f values are maintained quite constant during all the thermo-mechanical cycles at about 88 %. Moreover, the addition of the nanoclays did not affect the optimum results for R_r and R_f values presented by the neat blends in the heating responsiveness of these blends. Besides, also the samples containing 50 % of TPS reached high values in the latest cycles demonstrating

that also with the highest TPS content the shape memory properties of EVA are extraordinary.

Table 3. Values of R_r and R_f for the thermally-activated shape memory test for all the samples studied. Adapted with permission from (Sessini V, Raquez J-M, Lo Re G, et al. Multiresponsive Shape Memory Blends and Nanocomposites Based on Starch. ACS applied materials & interfaces. 2016 2016/08/03;8(30):19197-19201) [40]. Copyright 2016 American Chemical Society.

Sample		**R_r (%)**				**R_f (%)**			
	Cycle	1	2	3	4	1	2	3	4
EVA		94	97	97	100	99	86	89	85
B40TPS		100	100	99	100	89	87	89	87
B40TPS + 1 % $CLNa^+$		98	96	97	100	91	91	88	88
B50TPS		82	99	98	100	92	89	87	90
B50TPS + 1 % $CLNa^+$		81	90	100	100	93	91	89	87

The analysis of the strain energy involved in the shape memory experiments was carried out for all the samples following the same procedure reported previously [58]. In fact, the strain energy of an ideal shape memory polymer was estimated taking into account that the ε_u overlaps with ε_m in the stress-strain curves, and that an ideal material is able to recover all the applied deformation. Thus, based on this hypothesis, we were able to calculate the ideal as well as the real strain energy of the samples. In Figure 12, the values of the strain energy and strain recovery ratio obtained during the different cycles are showed for all the samples.

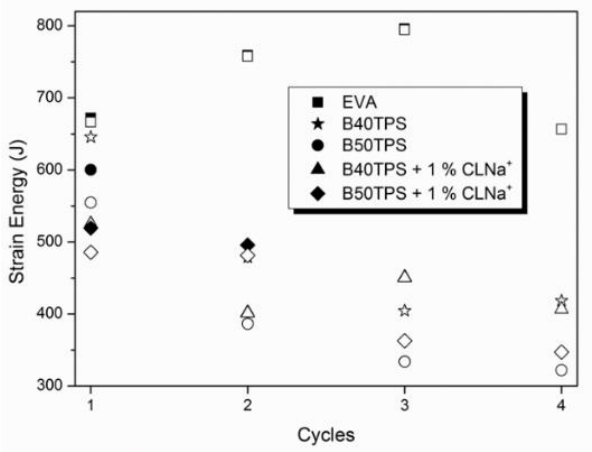

Figure 12. Strain energy for the different materials based on EVA/TPS blends.

The un-filled symbols in Figure 12 correspond to the real values and the filled ones to the ideal values. It is possible to note as the different symbols (filled and un-filled) are overlapped, thus in Table 4 the energy efficiency values are reported, as the ratio between the real and the ideal strain energies.

Table 4. The values obtained for the energy efficiency for all the samples.

Sample	**Energy Efficiency**			
	1	2	3	4
EVA	99.2	99.7	99.7	100.0
B40TPS	100.0	100.0	99.9	100.0
B40TPS + 1 % $CLNa^+$	99.9	99.7	99.8	100.0
B50TPS	92.4	99.9	99.9	100.0
B50TPS + 1 % $CLNa^+$	93.5	97.1	100.0	100.0

For all the samples the energy efficiency is very high after obtaining the better results for the sample B40TPS, showing values of 100 % also in the first cycle. Thus, the blends and their nanocomposites present behaviour almost ideal being capable to recover nearly all the deformation applied.

Poly(ethylene-co-vinyl acetate) random copolymer/starch nanocrystals nanocomposites.

Starch nanocrystals were synthesized by acid hydrolysis applying 100 rpm of mechanical stirring at 40 ºC, using a silicon oil bath, for 5 days. The final suspensions were washed by successive centrifugations in distilled until reaching neutral pH. Finally, it was freeze-dried to obtain SNCs powder.

Following the same mechanism and the same procedure used for EVA-based materials previously described, thermally-activated shape memory properties were studied for EVA reinforced with 2 wt % and 5 wt % of SNCs.

In order to study the effect of starch nanocrystals on the induced-crystallization mechanism of EVA, DSC analyses were performed at the same conditions of shape memory test. The DSC thermogram related to the first heating scan of non-stretched and stretched neat EVA and its nanocomposites are reported in Figure 13. Surprisingly, increasing the amount of SNCs on EVA matrix, the stretch-induced crystallization of the A crystal phase was inhibited. The thermograms showed as the melting enthalpy of the crystalline phase A peak decreased for stretched EVA-2SNC compared to that of stretched neat EVA and much more for stretched EVA-5SNC. Indeed, for EVA-5SNC the crystal phase A was almost absent although the sample was stretched at 250 % of elongation. Moreover, an increase of the melting enthalpy of crystalline phase B was observed in the nanocomposites.

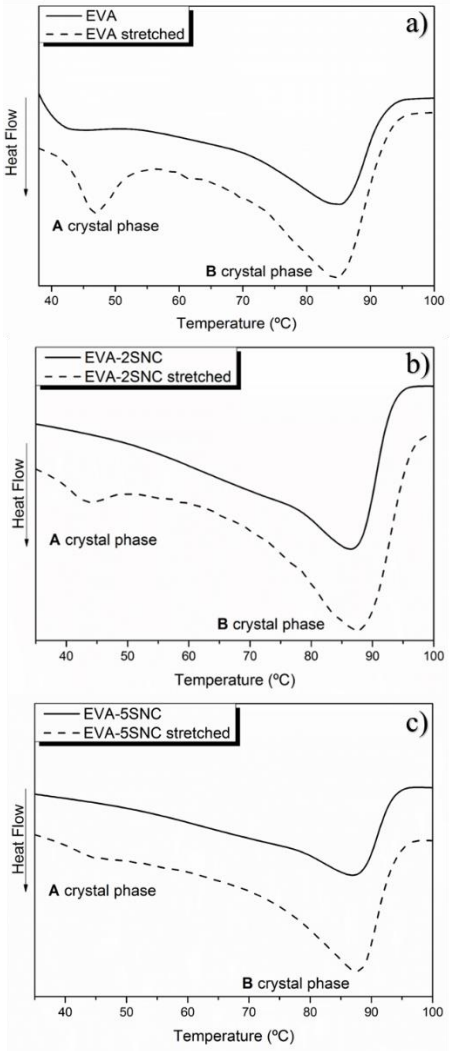

Figure 13. DSC thermogram of first scan of non-stretched and stretched neat EVA and its nanocomposites: a) Neat EVA, b) EVA-2SNC and c) EVA-5SNC. Adapted with permission from (Sessini V, Raquez J-M, Lo Re G, et al. Multiresponsive Shape Memory Blends and Nanocomposites Based on Starch. ACS applied materials & interfaces. 2016 2016/08/03;8(30):19197-19201) [40]. Copyright 2016 American Chemical Society.

This behaviour and the induced-crystallization of the crystalline phase B rather than the crystalline phase A was reflected in the shape memory results. The 2D stress-strain and 3D thermo-mechanical stress-strain-temperature cycle diagram are shown in Figure 14. In order to evaluate the repeatability of the shape-memory properties, different thermo-mechanical cycles were completed

for each sample. It was not possible to do more than 3 cycles because the EVA/SNC nanocomposites were broken.

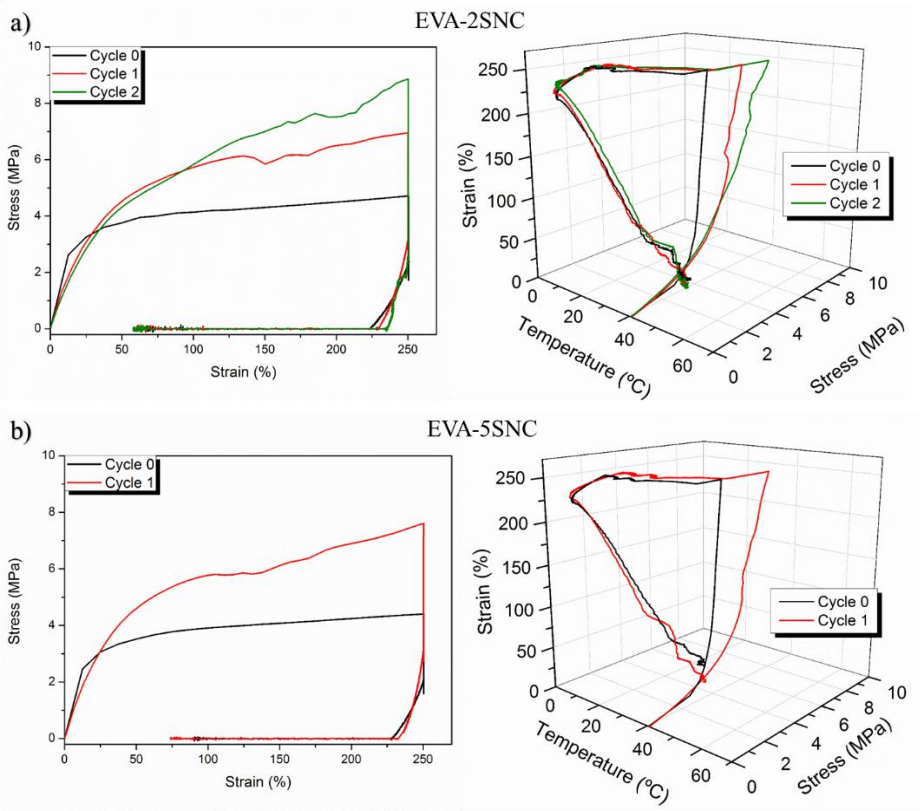

Figure 14. 2D stress-strain and 3D thermo-mechanical stress-strain-temperature cycle diagram for: a) EVA-2SNC and b) EVA-5SNC.

Observing Figure 14, it is easy to notice that after the cycle 0 (named 0 because is used to delete the thermal history of the materials and in general is not reported) the value of stress strongly increases. This is due to the progressive increase of the B crystal phase, which is able to fix more toughly the permanent network formed by amorphous EVA, SNCs and B crystal phase. The values obtained in every cycle for both the R_r and the R_f are summarized in Table 5. The results showed that the presence of SNCs affected the thermo-responsiveness of EVA based on induced-crystallization mechanism.

Table 5. Values of R_r and R_f for the thermally-activated shape memory test of the samples studied.

Sample	R_r (%)			R_f (%)		
	0	1	2	0	1	2
EVA	96	94	97	90	99	96
EVA-2SNC	73	77	77	92	94	96
EVA-5SNC	64	70	-	94	95	-

The values reflected that the ability to recover the initial shape decrease when the amount of SNCs increase into the EVA matrix, showing R_r values of 20 % less for EVA-2SNC and almost 30 % less for EVA-5SNC compared to neat EVA. Contrarily, the high EVA ability to fix the temporary shape did not undergo any significant change though the amount of SNCs increased into the EVA matrix.

FINAL REMARKS

In brief, shape memory polymers are a special class of smart materials capable to memorize and to recover, triggered by an external stimulus, their original shape from a temporary shape programmed by mechanical deformation.
This chapter focuses the attention on polymeric nanocomposite systems with shape memory response due to their scientific and technological relevance.
In particular three different systems were studied based on ethylene copolymers such as Nucrel® and Surlyn® reinforced with Silica nanoparticles, blends of EVA/thermoplastic starch reinforced with natural bentonite and EVA reinforced with SNCs. All of these systems present shape memory ability, evidencing how the addition of well dispersed nanoparticles can affect the shape memory response of the neat matrices.

ACKNOWLEDGEMENTS

Authors thank Spanish Ministry of Economy, Industry and Competitiveness, MINEICO, (MAT2017- 88123-P) and the Regional Government of Madrid (S2013/MIT-2862) for the economic support. L.P. acknowledges MINEICO for the “Ramon y Cajal” (RYC-2014-15595) contract. Authors thanks also CSIC for the I-LINK project, I-LINK1149. JMR is a FRS-FNRS research associate.

REFERENCES

1. Wei, Z., R. Sandstroröm, and S. Miyazaki, *Shape-memory materials and hybrid composites for smart systems: Part I Shape-memory materials.* Journal of Materials Science, 1998. 33(15): p. 3743-3762.

2. Koerner, H., et al., *Polymer design for high temperature shape memory: Low crosslink density polyimides.* Polymer, 2013. 54(1): p. 391-402.

3. Rousseau, I.A., *Challenges of shape memory polymers: A review of the progress toward overcoming SMP's limitations.* Polymer Engineering & Science, 2008. 48(11): p. 2075-2089.

4. Sessini, V., et al., *Humidity-Activated Shape Memory Effects on Thermoplastic Starch/EVA Blends and Their Compatibilized Nanocomposites.* Macromolecular Chemistry and Physics, 2017. 218(24).

5. Navarro-Baena, I., et al., *Design of biodegradable blends based on PLA and PCL: From morphological, thermal and mechanical studies to shape memory behavior.* Polymer degradation and stability, 2016. 132: p. 97-108.

6. Arrieta, M.P., V. Sessini, and L. Peponi, *Biodegradable poly(ester-urethane) incorporated with catechin with shape memory and antioxidant activity for food packaging.* European Polymer Journal, 2017. 94: p. 111-124.

7. Peponi, L. et al., *Thermally-activated shape memory effect on biodegradable nanocomposites based on PLA/PCL blends reinforced with hydroxyapatite.* Polymer degradation and stability, 2018, 10.1016/j.polymdegradstab.2018.02.019.

8. Wang, C.C., et al., *Cooling-/water-responsive shape memory hybrids.* Composites science and technology, 2012. 72(10): p. 1178-1182.

9. Sessini, V., et al., *Humidity-activated shape memory effect on plasticized starch-based biomaterials.* Carbohydrate polymers, 2018. 179: p. 93-99.

10. Lee, Y.M., S.H. Kim, and C.S. Cho, *Synthesis and swelling characteristics of pH and thermoresponsive interpenetrating polymer network hydrogel composed of poly (vinyl alcohol) and poly (acrylic acid).* Journal of Applied Polymer Science, 1996. 62(2): p. 301-311.

11. Lendlein, A., et al., *Light-induced shape-memory polymers.* Nature, 2005. 434(7035): p. 879.

12. Liu, Y., et al., *Review of electro-active shape-memory polymer composite.* Composites science and technology, 2009. 69(13): p. 2064-2068.

13. Navarro-Baena, I., J.M. Kenny, and L. Peponi, *Thermally-activated shape memory behaviour of bionanocomposites reinforced with cellulose nanocrystals.* Cellulose, 2014. 21(6): p. 4231-4246.

14. Odent, J., et al., *Ultra-stretchable ionic nanocomposites: From dynamic bonding to multi-responsive behavior.* Journal of Materials Chemistry A, 2017. 5(26): p. 13357-13363.

15. Odent, J., et al., *Shape-Memory Behavior of Polylactide/Silica Ionic Hybrids.* Macromolecules, 2017. 50(7): p. 2896-2905.

16. Mather, P.T., X. Luo, and I.A. Rousseau, *Shape memory polymer research.* Annual Review of Materials Research, 2009. 39: p. 445-471.

17. Heuchel, M., et al., *Relaxation based modeling of tunable shape recovery kinetics observed under isothermal conditions for amorphous shape-memory polymers.* Polymer, 2010. 51(26): p. 6212-6218.

18. Karger-Kocsis, J., *Biodegradable polyester-based shape memory polymers: Concepts of (supra) molecular architecturing.* Express Polymer Letters, 2014. 8(6): p. 397-412.

19. Olalla, A., et al., *Smart Nanocellulose Composites With Shape-Memory Behavior*, in *Multifunctional Polymeric Nanocomposites Based on Cellulosic Reinforcements*2016, Elsevier. p. 277-312.

20. Peponi, L., I. Navarro-Baena, and J. Kenny, *Shape memory polymers: properties, synthesis and applications*, in *Smart polymers and their applications*2014, Elsevier. p. 204-236.

21. Bellin, I., S. Kelch, and A. Lendlein, *Dual-shape properties of triple-shape polymer networks with crystallizable network segments and grafted side chains.* Journal of Materials Chemistry, 2007. 17(28): p. 2885-2891.

22. Lendlein, A. and S. Kelch, *Shape-memory polymers.* Angewandte Chemie International Edition, 2002. 41(12): p. 2034-2057.

23. Pandini, S., et al., *One-way and two-way shape memory behaviour of semi-crystalline networks based on sol–gel cross-linked poly (ε-caprolactone).* Polymer, 2013. 54(16): p. 4253-4265.

24. Luo, H., et al., *Novel Biodegradable Shape Memory Material Based on Partial Inclusion Complex Formation between α-Cyclodextrin and Poly (ε-caprolactone).* Biomacromolecules, 2008. 9(10): p. 2573-2577.

25. Tan, L.-S. and D.H. Wang, *Multifunctional crosslinkers for shape-memory polyimides, polyamides and poly (amide-imides) and methods of making the same*, 2015, Google Patents.

26. Gordon, M. and J.S. Taylor, *Ideal copolymers and the second-order transitions of synthetic rubbers. I. Non-crystalline copolymers.* Journal of Chemical Technology and Biotechnology, 1952. 2(9): p. 493-500.

27. Pilate, F., et al., *Shape-memory polymers for multiple applications in the materials world.* European Polymer Journal, 2016. 80: p. 268-294.

28. Bidsorkhi, H.C., et al., *Preparation and characterization of ethylene-vinyl acetate/halloysite nanotube nanocomposites.* Journal of Materials Science, 2015. 50(8): p. 3237-3245.

29. Peponi, L., et al., *Processing of nanostructured polymers and advanced polymeric based nanocomposites.* Materials Science and Engineering R: Reports, 2014. 85(1): p. 1-46.

30. Sessini, V., et al., *Processing of edible films based on nanoreinforced gelatinized starch.* Polymer degradation and stability, 2016. 132: p. 157-168.

31. Sonseca, Á., et al., *Mechanical and shape-memory properties of poly(mannitol sebacate)/cellulose nanocrystal nanocomposites.* Journal of Polymer Science, Part A: Polymer Chemistry, 2014. 52(21): p. 3123-3133.

32. Mujica-Garcia, A., et al., *Poly (lactic acid) melt-spun fibers reinforced with functionalized cellulose nanocrystals.* RSC Advances, 2016. 6(11): p. 9221-9231.

33. Peponi, L., et al., *Smart Polymers*, in *Modification of Polymer Properties*2016. p. 131-154.

34. Rajisha, K., et al., *Preparation and characterization of potato starch nanocrystal reinforced natural rubber nanocomposites.* International journal of biological macromolecules, 2014. 67: p. 147-153.

35. Chen, Y., et al., *Comparative study on the films of poly (vinyl alcohol)/pea starch nanocrystals and poly (vinyl alcohol)/native pea starch.* Carbohydrate polymers, 2008. 73(1): p. 8-17.

36. Li, X., et al., *Mechanical, barrier and morphological properties of starch nanocrystals-reinforced pea starch films.* Carbohydrate polymers, 2015. 121: p. 155-162.

37. Darder, M., P. Aranda, and E. Ruiz-Hitzky, *Bionanocomposites: a new concept of ecological, bioinspired, and functional hybrid materials.* Advanced Materials, 2007. 19(10): p. 1309-1319.

38. Henderson, A.M., *Ethylene-vinyl acetate (EVA) copolymers: a general review.* IEEE Electrical Insulation Magazine, 1993. 9(1): p. 30-38.

39. Alakrach, A., et al. *Thermal properties of ethyl vinyl acetate (EVA)/montmorillonite (MMT) nanocomposites for biomedical applications*. in *MATEC Web of Conferences*. 2016. EDP Sciences.

40. Sessini, V., et al., *Multiresponsive Shape Memory Blends and Nanocomposites Based on Starch.* ACS applied materials & interfaces, 2016. 8(30): p. 19197-19201.

41. Nöchel, U., et al., *Triple-Shape Effect with Adjustable Switching Temperatures in Crosslinked Poly [ethylene-co-(vinyl acetate)].* Macromolecular Chemistry and Physics, 2014. 215(24): p. 2446-2456.

42. Li, F., et al., *Shape memory effect of ethylene–vinyl acetate copolymers.* Journal of Applied Polymer Science, 1999. 71(7): p. 1063-1070.

43. Li, J., W.R. Rodgers, and T. Xie, *Semi-crystalline two-way shape memory elastomer.* Polymer, 2011. 52(23): p. 5320-5325.

44. Wu, X., W. Huang, and H. Tan, *Characterization of shape recovery via creeping and shape memory effect in ether-vinyl acetate copolymer (EVA).* Journal of Polymer Research, 2013. 20(8): p. 150.

45. Gao, F., G. Beyer, and Q. Yuan, *A mechanistic study of fire retardancy of carbon nanotube/ethylene vinyl acetate copolymers and their clay composites.* Polymer degradation and stability, 2005. 89(3): p. 559-564.

46. Sengupta, R., et al., *A review on the mechanical and electrical properties of graphite and modified graphite reinforced polymer composites.* Progress in polymer science, 2011. 36(5): p. 638-670.

47. Bidsorkhi, H.C., et al., *Mechanical, thermal and flammability properties of ethylene-vinyl acetate (EVA)/sepiolite nanocomposites.* Polymer Testing, 2014. 37: p. 117-122.

48. Zanetti, M., et al., *Synthesis and thermal behaviour of layered silicate–EVA nanocomposites.* Polymer, 2001. 42(10): p. 4501-4507.

49. Morlat-Therias, S., et al., *Polymer/carbon nanotube nanocomposites: influence of carbon nanotubes on EVA photodegradation.* Polymer degradation and stability, 2007. 92(10): p. 1873-1882.

50. Varley, R.J., S. Shen, and S. van der Zwaag, *The effect of cluster plasticisation on the self healing behaviour of ionomers.* Polymer, 2010. 51(3): p. 679-686.

51. Varley, R.J. and S. van der Zwaag, *Towards an understanding of thermally activated self-healing of an ionomer system during ballistic penetration.* Acta Materialia, 2008. 56(19): p. 5737-5750.

52. Francesconi, A., et al., *Comparison of self-healing ionomer to aluminium-alloy bumpers for protecting spacecraft equipment from space debris impacts.* Advances in Space Research, 2013. 51(5): p. 930-940.

53. Lewis, C.L. and E.M. Dell, *A review of shape memory polymers bearing reversible binding groups.* Journal of Polymer Science Part B: Polymer Physics, 2016. 54(14): p. 1340-1364.

54. Eisenberg, A. and M. Navratil, *Ion clustering and viscoelastic relaxation in styrene-based ionomers. IV. X-ray and dynamic mechanical studies.* Macromolecules, 1974. 7(1): p. 90-94.

55. Tachino, H., et al., *Dynamic mechanical relaxations of ethylene ionomers.* Macromolecules, 1993. 26(4): p. 752-757.

56. Wakabayashi, K. and R.A. Register, *Morphological origin of the multistep relaxation behavior in semicrystalline ethylene/methacrylic acid ionomers.* Macromolecules, 2006. 39(3): p. 1079-1086.

57. Zhao, Z., et al., *Three-Dimensional Printed Shape Memory Objects Based on an Olefin Ionomer of Zinc-Neutralized Poly (ethylene-co-methacrylic acid).* ACS applied materials & interfaces, 2017. 9(32): p. 27239-27249.

58. Peponi, L., et al., *Synthesis and characterization of PCL–PLLA polyurethane with shape memory behavior.* European Polymer Journal, 2013. 49(4): p. 893-903.